Supplemental Material for:
"Decomposition and terapascal phases of water ice"

Chris J. Pickard, Miguel Martinez-Canales, and R. J. Needs

ENTHALPY-PRESSURE DIAGRAM (WITHOUT NUCLEAR ZERO POINT MOTION)

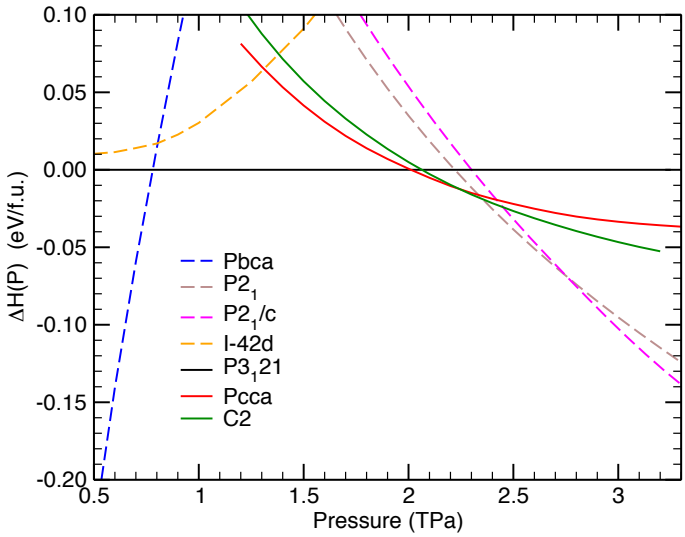

FIG. 1. Variation of the enthalpies with pressure for high-pressure water-ice structures. Previously-known structures are indicated by dashed lines and solid lines are used for the phases we have found. Nuclear zero-point (ZP) motion is not included.

The vibrational contribution to the enthalpy has a very significant influence on the stability regions of the H_2O phases.

Fig. 1 shown above gives the DFT enthalpy-pressure diagram without nuclear zero-point motion effects. This figure complements Fig. 1 of the main text, which shows a similar graph, but including nuclear zero point motion effects. The phase transition pressures given in Table 1 of the main text match those of Fig. 1. The pressure used for calculating the Gibbs Free Energy and displayed in all figures of the main text includes the vibrational contribution within the quasi-harmonic approximation (QHA). In other words:

$$P(V,T) = -\frac{\partial F(V,T)}{\partial V} \approx -\frac{\partial E_{\rm dft}(V)}{\partial V} - \frac{\partial F_{\rm vibr}(V,T)}{\partial V}$$

LOCAL DENSITY APPROXIMATION (LDA) CALCULATIONS

We performed calculations for the $Pbca$, $P3_121$, $P2_1/c$ and $C2/m$ phases with the same computational parameters as for the data in Fig. 1, but with the LDA functional [4] instead of PBE. The PBE and LDA results for the $Pbca \leftrightarrow P3_121$ and $P2_1/c \leftrightarrow C2/m$ transition pressures are similar. We found transition pressures for the $Pbca \leftrightarrow P3_121$ transition of 0.78 TPa (PBE) and 0.69 TPa (LDA), and for the $P2_1/c \leftrightarrow C2/m$ transition we found 6.06 (PBE) and 6.59 TPa (LDA). The fractional difference between the PBE and LDA transition pressures, given by |P(LDA)-P(PBE)|/P(PBE), is equal to 0.12 for $Pbca \leftrightarrow P3_121$ and 0.09 for $P2_1/c \leftrightarrow C2/m$. The fractional difference in the transition pressures is therefore smaller at the higher-pressure transition.

DENSITIES OF ICE PHASES

P (TPa)	Phase	density (g/cm^3)
0	ordered-Ih	0.917 (expt)
0.1	ice X	3.18
0.5	$Pbcm$	4.87
0.8	$Pbca$	5.70
1.0	$P3_121$	6.29
2.0	$Pcca$	8.16
2.25	$C2$	8.55
2.5	$P2_1$	8.94
3.25	$P2_1/c$	9.93
6.0	$C2/m$	12.84

TABLE I. Densities of various ice phases. The chosen pressures reflect the thermodynamically stable regions of the various phases.

ANALYSIS OF REDUCED DENSITY GRADIENTS

	C-dia (0 GPa)	Si-dia (0 GPa)	α-quartz (0 GPa)	Cubic H_2O (0 GPa)	$P3_121$ H_2O (1 TPa)	$C2/m$ H_2O (6 TPa)
Median	0.543	0.635	1.033	1.898	0.476	0.330
Mean	0.511	0.611	1.046	1.876	0.450	0.312
Max.	0.858	1.175	2.276	4.601	0.734	0.510

TABLE II. Median, mean and maximum reduced density gradients obtained from pseudopotential calculations in which the 1s electrons are treated as core, for carbon and silicon in the diamond structure, α quartz (SiO_2), and cubic ice (zero pressure), and for the $P3_121$ and $C2/m$ structures of H_2O at pressures of 1 TPa and 6 TPa, respectively.

The reduced density gradient of a non-spin-polarized system is defined as

$$s(\mathbf{r}) = \frac{|\nabla n(\mathbf{r})|}{2(3\pi^2)^{1/3}(n(\mathbf{r}))^{4/3}},$$

where $n(\mathbf{r})$ is the charge density. $s(\mathbf{r})$ can be used to quantify the non-uniformity of the electronic charge density, in the sense that smaller values of $s(\mathbf{r})$ indicate that the gradient terms in density functional such as PBE are less important.

The data in Table II shows reduced density gradients for the pseudo-valence charge densities of C, Si and H_2O structures. The median and mean reduced densities are very similar for each system. C-dia and Si-dia show the smallest median, mean and maximum reduced density gradients at zero pressure, while those of α quartz are roughly two times larger, and those of cubic H_2O are roughly four times larger. Cubic ice exhibits the largest median, mean, and maximum mean values of $s(\mathbf{r})$ for the six systems studied. The systems with the smallest median, mean, and maximum values of $s(\mathbf{r})$ are the high pressure $P3_121$ and $C2/m$ phases of H_2O.

We note that the PBE functional gives very good descriptions of C-dia and Si-dia at zero pressure. We therefore expect that PBE works even better for the two high-pressure ice phases than for C-dia and Si-dia at zero pressure. Our data suggests that cubic ice at zero pressure is the furthest of these systems from the uniform limit, while the high pressure $P3_121$ and $C2/m$ phases of H_2O are closest to the uniform limit. The LDA and PBE density functionals are well suited for studying sp bonded systems with relatively small reduced density gradients, as they obey the uniform limit and give a good account of the linear response of the electron gas to an external potential. Our data support the idea that the LDA and PBE density functionals give a better description of high pressure phases of H_2O such as $P3_121$ and $C2/m$ than of low pressure phases such as cubic ice.

PICTURES AND DATA FOR SELECTED STRUCTURES

In order to aid the reproducibility of our results, we include the structural data for the new phases considered. These data are supplied as CIF datafiles. Fig. 2 shows some further visualisations of our new ice phases.

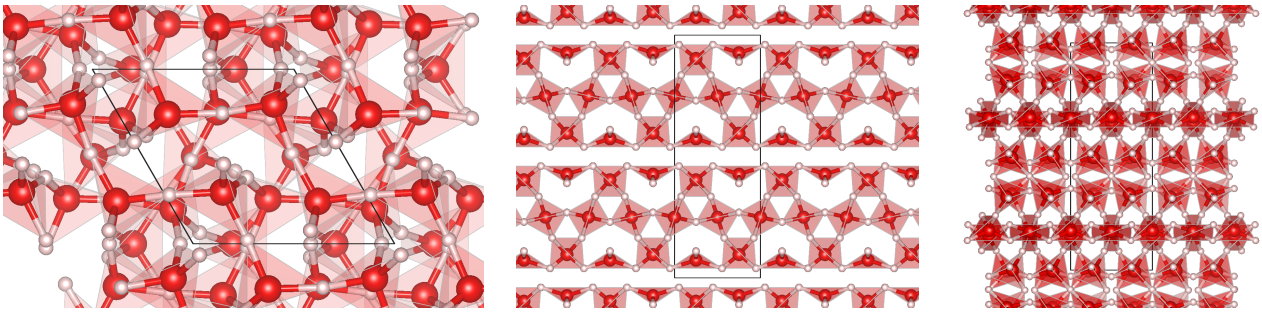

FIG. 2. *(left)* The $P3_12_1$ structure of water ice at 1 TPa, *(center)* the *Pcca* structure of water ice at 2.25 TPa and *(right)* the $C2$ structure at 2 TPa. The O atoms are shown in red and the H atoms in gray. The translucent tetrahedra are used to highlight 4-fold coordination.

ADDITIONAL DETAILS OF THE CALCULATIONS

The searches

Searches for H_2O structures were performed at 1.5, 2.5, 4, 5, 6, 10 and 20 TPa. For the other compositions, the searches at 1.5 and 2.5 TPa were omitted. Extensive use was made of symmetry constraints, but for H_2O unconstrained searches with up to 12 fu were performed.

Ultrasoft pseudopotentials

For the searches at 1.5 and 2.5 TPa we used pseudopotential core radii of R_c(H)=0.8 a.u. and R_c(O)=1.3 a.u., while for higher pressures harder pseudopotentials were used, R_c(H)=0.6 a.u. and R_c(O)=1.0 a.u. The enthalpy data for the H_2O phases were generated using the softer pseudopotentials, while the decomposition of H_2O at higher pressures was studied using the harder potential. A still harder potential with R_c(H)=0.4 a.u. and R_c(O)=0.8 a.u. was tested for the highest pressures investigated, as well as an all-electron pseudopotential for O. These even more accurate calculations did not significantly alter our results.

Basis sets and Brillouin zone integrations

For the searches at 1.5 and 2.5 TPa we used a plane wave cut-off energy of 340 eV and a Monkhorst-Pack [1] Brillouin zone sampling grid of spacing $2\pi \times 0.1$ Å^{-1}. The searches at higher pressures were performed with a plane wave cut-off energy of 790 eV and a Monkhorst-Pack Brillouin zone sampling grid of spacing $2\pi \times 0.1$ Å^{-1}.

The enthalpy data for the H_2O phases were generated using a plane wave cut-off energy of 590 eV and a Brillouin zone sampling grid of spacing $2\pi \times 0.07$ Å^{-1}. The decomposition of H_2O, as reported in the convex hull plots of the main paper, was studied using a plane wave cut-off energy of 950 eV and a Brillouin zone sampling grid of spacing $2\pi \times 0.07$ Å^{-1}.

ELECTRONIC PROPERTIES OF THE PHASES

Variation of the band gaps of the phases with pressure

The calculated band gap of water ice initially increases as pressure is applied, reaching a maximum value of about 10 eV at the transition from Ice X to *Pbcm* at about 290 GPa. At higher pressures the band gaps decline with pressure. Metallization of H_2O occurs at the transition to the $C2/m$ phase, as reported in Ref. 2.

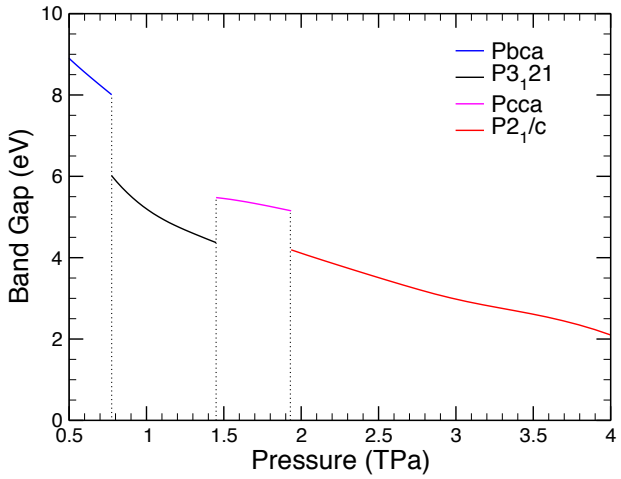

FIG. 3. Band gaps of phases of water ice at TPa pressures. The band gap values are shown only within the regions in which the phases are thermodynamically stable.

Electronic properties of the $H_{2+\delta}O$ structures

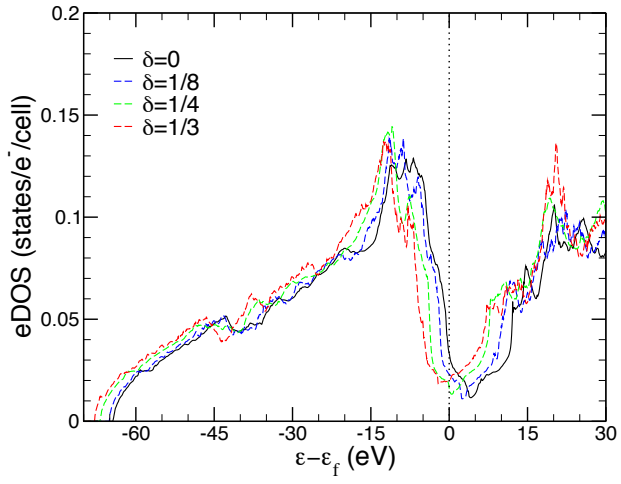

FIG. 4. Electronic densities of states (eDos) of $H_{2+\delta}O$ structures at 6 TPa. The form of the eDos does not vary greatly with δ, but the curves are shifted downwards with respect to the Fermi energy as δ increases. Note that the eDos at the Fermi energy takes its minimum value at $\delta = 1/4$, which corresponds to the minimum in the convex hull shown in Fig. 4(a) of the main text.

LATTICE DYNAMICS

The phonon calculations were performed using the Quantum ESPRESSO code [3]. For the phonon calculations under 4 TPa we used a PAW pseudopotential with R_c(O)=1.2 a.u. and R_c(H)=0.8 a.u. Suitable energy convergence was achieved using a plane wave cut-off energy of 60 Ry (816 eV), an augmentation charge cutoff of 400 Ry and Brillouin zone sampling grids of spacing $2\pi \times 0.03$ Å^{-1}.

In the higher pressure calculations for H_2O_2 and $C2/m$ we used the same pseudopotential settings as in the CASTEP calculations with the harder pseudopotentials. We performed the calculations using 125 and 1250 Ry energy cut-offs for the wavefunctions and charge densities, respectively.

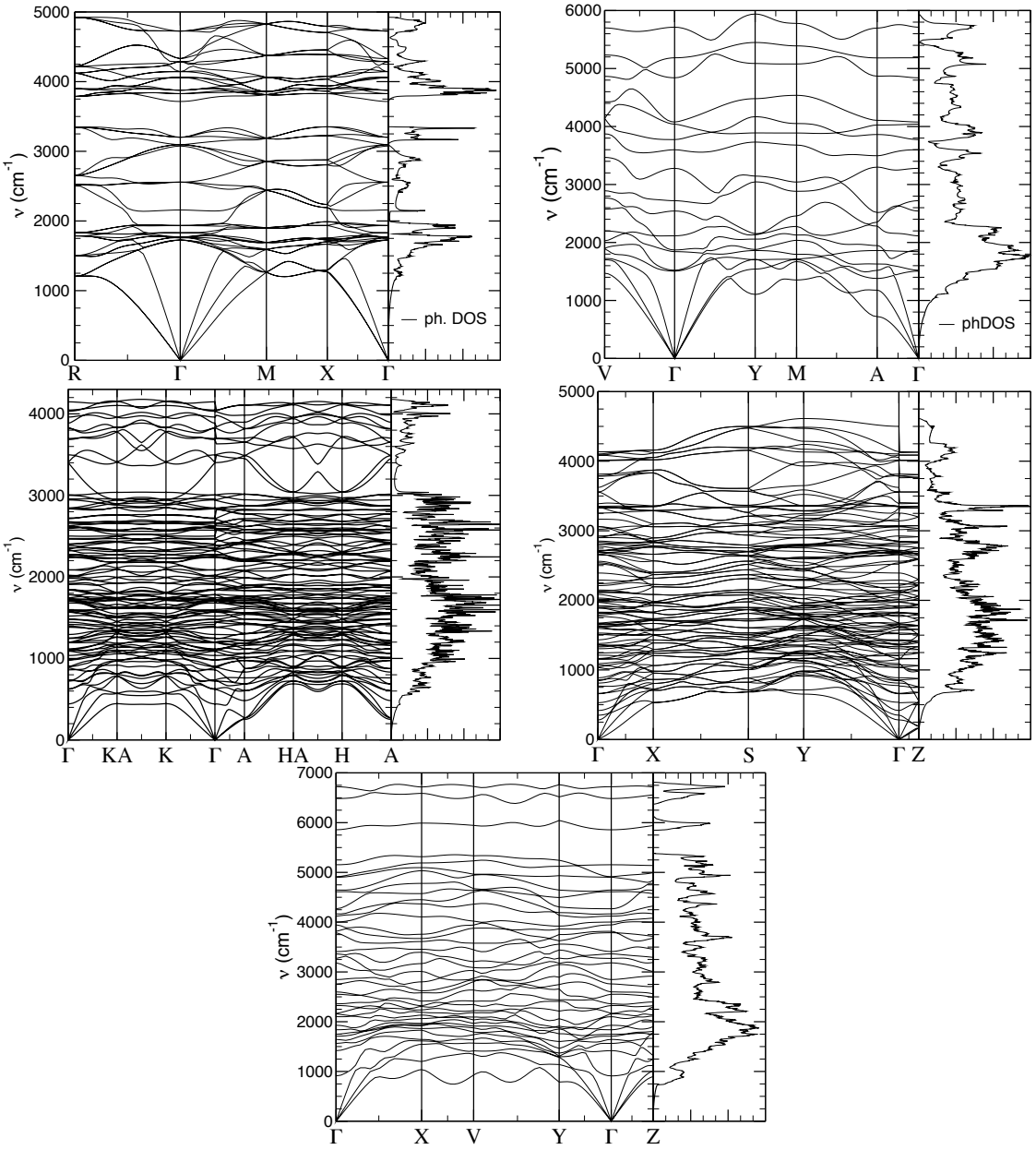

FIG. 5. (a) Phonon dispersion relations of the $Pa\bar{3}$ structure of H_2O_2 at 6 TPa, (b) $C2/m$ H_2O at 5 TPa, (c) $P3_121$ at 1 TPa, (d) $Pcca$ at 1.6 TPa, and (e) $H_{2+\delta}O$ with $\delta = 1/4$ at 6 TPa. The phonon modes are found to be stable in each case.

[1] H. J. Monkhorst and J. D. Pack, Phys. Rev. B **13**, 5188 (1976).
[2] J. M. McMahon, Phys. Rev. B **84**, 220104 (2011).
[3] P. Giannozzi *et al.*, J. Phys.: Condens. Matter **21**, 395502 (2009). http://arxiv.org/abs/0906.2569.
[4] J. P. Perdew and A. Zunger, Phys. Rev. B **23**, 5048 (1981).